Electrochimica Acta 69 (2012) 295–300

Contents lists available at SciVerse ScienceDirect

Electrochimica Acta

journal homepage: www.elsevier.com/locate/electacta

Manganese dioxide nanotube and nitrogen-doped carbon nanotube based composite bifunctional catalyst for rechargeable zinc-air battery

Zhu Chen, Aiping Yu, Raihan Ahmed, Haijiang Wang, Hui Li, Zhongwei Chen*

Department of Chemical Engineering, Waterloo Institute for Nanotechnology, Waterloo Institute for Sustainable Energy, University of Waterloo, Waterloo, ON, Canada N2L 3G1

ARTICLE INFO

Article history:
Received 11 January 2012
Received in revised form 1 March 2012
Accepted 1 March 2012
Available online 9 March 2012

Keywords:
Nitrogen-doped carbon nanotubes
Manganese dioxide nanotubes
Oxygen reduction reaction
Oxygen evolution reaction
Bifunctional catalysts
Rechargeable zinc-air battery

ABSTRACT

A composite bifunctional catalyst (MnO_2–NCNT) was prepared from manganese dioxide (MnO_2) nanotubes and nitrogen-doped carbon nanotubes (NCNT) for the purpose of oxygen reduction (ORR) and evolution (OER) catalysis in the rechargeable zinc-air battery. From the half cell test, the MnO_2–NCNT composite illustrated excellent activities towards ORR and OER in alkaline conditions. Based on the battery test, the composite catalyst displayed outstanding discharge and charge performance while maintaining good stability. In both cases, the marked performance improvements from MnO_2–NCNT compared favourably to the NCNT and MnO_2, which are the constituents of the composite. In particular, MnO_2–NCNT exhibited improved half wave potential by 220 mV compared to MnO_2 and much superior OER stability compared to NCNT based on the rotating ring disk voltammetry results. According to battery test, MnO_2–NCNT decrease the battery resistance by 34% and concurrently improved the durability, discharge and charge performance in comparison to the MnO_2 nanotubes.

1. Introduction

Electrochemical devices such as fuel cell, battery and supercapacitors are potential alternatives for energy conversion and storage apart from the burning of fossil fuels. Among the different energy storage systems, the rechargeable zinc-air battery displays great promise due to many attractive features; for example, high energy density, cost-effective and environmentally friendly design, as well as low operating risks [1]. The excellent properties of rechargeable zinc-air batteries lead to potential applications in areas, such as stationary and portable power applications including electric vehicles [2,3]. In a rechargeable zinc-air battery, oxygen evolution (OER) and oxygen reduction (ORR) reactions occur on the air electrode during battery charge and discharge, respectively. The sluggish reaction kinetics and large overpotential associated with OER and ORR greatly limit the performance of rechargeable zinc-air batteries [2,4]. Bifunctional catalysts can greatly improve the kinetics of OER and ORR making it the most critical determining factor to the performance and lifetime of the battery [2]. As a result, an affordable, active and stable bifunctional catalyst is in great demands to improve to the performance of rechargeable zinc-air batteries.

Currently, the most effective bifunctional catalysts are based on precious metals, for example, Pt-IrO_2 and PtIrRu [5,6]. However, the high cost and scarcity of the precious metals greatly hinder the large scale implementation. Non-precious metal catalysts including mixed metal oxides with perovskite [7], or spinel [8] structures have been studied extensively, however further improvements to the performance are required before successful commercialization. Recently, perovskite oxide has been combined with nitrogen doped carbon nanotube (NCNT) in a core-corona fashion to produce bifunctional catalyst with excellent activity and stability [9]. In this paper, similar idea is explored where transition metal oxides and NCNT will be integrated. Transition metal oxides, in particular, the manganese oxide, has demonstrated great potential due to high ORR activity [10,11] and low cost. Furthermore, manganese oxide is an appealing candidate of bifunctional catalyst for air electrode based on previously documented OER activity [12]. Nevertheless, the poor electrical conductivity of manganese oxide greatly inhibits the catalyst performance in term of high electrical resistance. This problem can be mitigated through the use of different catalyst supports such as graphene and carbon nanotubes [13,14]. Using catalyst supports, increase performance and stability of MnO_2 could be achieved similar to the commercial carbon supported platinum catalyst in polymer electrolyte membrane (PEM) fuel cell [15,16]. Recently, NCNT has been used as catalyst support which enhanced the performance of the cathode catalyst in PEM fuel cell [17–19]. Similar to many other non-precious metal catalysts [20–22], NCNT has shown ORR activity comparable to that of Pt/C in alkaline conditions [19–25], which leads to recent applications in the air cathode

* Corresponding author. Tel.: +1 519 888 4567x38664; fax: +1 519 746 4979.
E-mail address: zhwchen@uwaterloo.ca (Z. Chen).

0013-4686/$ – see front matter © 2012 Elsevier Ltd. All rights reserved.
doi:10.1016/j.electacta.2012.03.001

of zinc air battery [26]. As a result, combining NCNT and MnO_2 could be beneficial in two-folds, where improvements to the electrical conductivity and the overall activity of the manganese oxide are expected. In this paper, we report the preparation of a composite bifunctional catalyst—MnO_2–NCNT by simple mixing of MnO_2 nanotube and NCNT. The catalytic performance towards ORR and OER was evaluated in a home-made zinc-air battery under alkaline conditions. The contribution of NCNT catalyst towards the performance of the composite was evaluated, and it is compared to that of pure MnO_2 to assess the potential use of MnO_2–NCNT as the air electrode catalyst for rechargeable zinc-air batteries.

2. Experimental methods

MnO_2 nanotubes were synthesized by a hydrothermal treatment at 140 °C for 12 h. The sample was washed with de-ionized water and dried overnight before use. NCNT was prepared by chemical vapour deposition of a precursor admixture containing ethylenediamine (99%, Aldrich) and ferrocene (98%, Aldrich), at 700 °C under N_2 protection in a horizontal tube furnace. The MnO_2–NCNT was prepared by mixing the MnO_2 nanotube and NCNT in 1:1 weight ratio in ethanol followed by drying in oven.

To characterize the pure MnO_2 and MnO_2–NCNT composite, scanning electron microscopy (SEM) (JEOL, Leo 1530) was used to examine the morphology of the catalysts. X-ray diffraction (XRD) (Bruker AXS D8 Advance) was used to study the crystallography structure of the MnO_2 nanotubes and X-ray photoelectron spectroscopy (XPS) was used to investigate the surface elemental composition of the NCNTs. The electrocatalytic activity and stability of the catalyst were measured using rotating ring disk electrode (RRDE) voltammetry, which employed a bipotentiostat (Pine Instrument Co., AFCBP1) and a rotation speed controller (Pine Instrument Co., AFMSRCE). Battery test was conducted using a multichannel potentiostat (Princeton Applied Research, VersaSTAT MC) and a home-made zinc-air battery.

Prior to the RRDE voltammetry, 0.5 wt.% Nafion solution was prepared by dilution of 15 wt.% Nafion stock solution from Ion Power Inc. (Liquion Solution LQ-1115 1100EW 15 wt.%). This solution was used to prepare the catalyst ink by adding to it 4 mg of catalyst and sonicating to homogenous dispersion. The working electrode was deposited with 20 μL of catalyst ink, and once dried, immersed into a glass cell containing 0.1 M KOH electrolyte. A double junction Ag/AgCl reference and a platinum wire were employed as the reference and counter electrodes, respectively. ORR experiments were carried out in O_2 saturated electrolyte with different electrode rotation speeds, and the background measurements were performed in N_2 saturated electrolyte solution without electrode rotation. The potential range of ORR and background measurements was from −1 to 0.2 V vs. Ag/AgCl at a scan rate of 10 mV/s. The capacitive current was measured by the cyclic voltammetry (CV) method in N_2 saturated electrolyte solution and the potential was swept from −1 to 0.2 V at 50 mV/s. The evaluation of OER catalysis was performed in N_2 saturated electrolyte and the working electrode potential was swept from 0 to 1 V at 50 mV/s. In addition, the electrode was rotated at 900 rpm to remove the evolved O_2 from surface of the electrode during the OER test.

Prior to the battery test, the air electrode was prepared by spraying the catalyst on to a gas diffusion layer (Ion Power Inc., SGL Carbon 10 BB, 2.5 cm × 2.5 cm) to achieve catalyst loading of 0.5 $mg_{catalyst}/cm^2$. The electrolyte used in the zinc-air battery was 6 M KOH, and a polished zinc plate was used as the anode. Galvanodynamic method was used to discharge or charge the battery from 0 to 200 mA. Battery cycling experiments were performed using the recurrent galvanic pulse method, where one cycle consisted of a discharge step at 50 mA for 300 s followed by a charging step of the same current and duration. Impedance measurements were carried out from 100 kHz to 0.1 Hz while applying an AC potential of 20 mV.

3. Results and discussion

SEM and TEM techniques were used to investigate the morphology of the MnO_2 nanotubes and NCNT. The tubular structures of MnO_2 and the bamboo compartments of NCNT are clearly shown in Fig. 1. Based on the SEM image, the diameter of MnO_2 nanotube is estimated to be approximately 100 nm and the diameter of the NCNT is about 20-50 nm. XRD pattern of MnO_2 nanotubes (Fig. 1c) confirms the alpha-MnO_2 structure (JCPDS: 44-0141), which has been proposed to be favourable for ORR in the past [10]. The surface nitrogen content of NCNT is approximately 4 at.% according to the XPS analysis (Fig. 1d). The nitrogen content and the surface morphology of the NCNT have been reported to correlate with ORR activity and stability in alkaline conditions [27,28].

The electrochemical behaviours of the catalysts towards ORR and OER in half cell setup were evaluated using RRDE voltammetry (Fig. 2). Based on the voltammetry results, a significant positive shift (+0.22 V) in the half wave potential and a doubled limiting current density are observed for the MnO_2–NCNT in comparison to the pure MnO_2 (Fig. 2a). The marked enhancements in the half cell performance observed for the MnO_2–NCNT composite can be attributed to the higher electrical conductivity as a consequence of NCNT addition. The effect of support on the performance of MnO_2 catalyst has been investigated where the addition of carbon support drastically improves the performance of the catalyst [11,29]. Furthermore, NCNT has been reported to be an efficient ORR catalyst via the four electron transfer reaction pathway [30]. The incorporation of NCNT in the composite catalyst not only improves the electrical conductivity, but also the overall activity for ORR catalysis. Besides the ORR activity, excellent OER activity and stability are particularly critical for bifunctional catalysts. Poor OER performance of NCNT is immediately apparent in Fig. 2b, where 94% decrease in current density at 1 V is observed after 50 cycles. The fast degradation associated with NCNT is in sharp contrast to the stable OER behaviour of pure MnO_2 nanotube, where only 3% decrease in current density is observed (Fig. 2b). However, the obvious disadvantage of pure MnO_2 is the low current density obtained at 1 V. In order to simultaneously achieve high electrical conductivity and OER stability, NCNT was added to the MnO_2 nanotubes to obtain the MnO_2–NCNT composite material, and the advantage is evident through Fig. 2. The MnO_2–NCNT composite has retained 96% of the OER current density at 1 V after 50 cycles, which is drastically higher compared to NCNT (only 4% remained) indicating excellent OER stability of the composite material (Fig. 2b). Additionally, the MnO_2–NCNT compared demonstrates 7.4 times higher OER current density in comparison to the pure MnO_2. Excellent OER stability and current density have been exhibited by the MnO_2–NCNT composite, which suggest high catalyst activity and stability during charge operation of the battery.

The Koutecky–Levich (K–L) plots were constructed for potentials from −0.5 V to −0.65 V (Fig. 3b and d) using the following equation,

$$\frac{1}{j} = \frac{1}{j_k} + \frac{1}{B\sqrt{\omega}} \quad (1)$$

where j_k is the kinetic current density, B is the Levich slope, ω is the rotation speed and j is the observed current density. The Levich slope can be further defined as:

$$B = 0.62nFC_{O_2}D_{O_2}^{2/3}\upsilon^{-1/6} \quad (2)$$

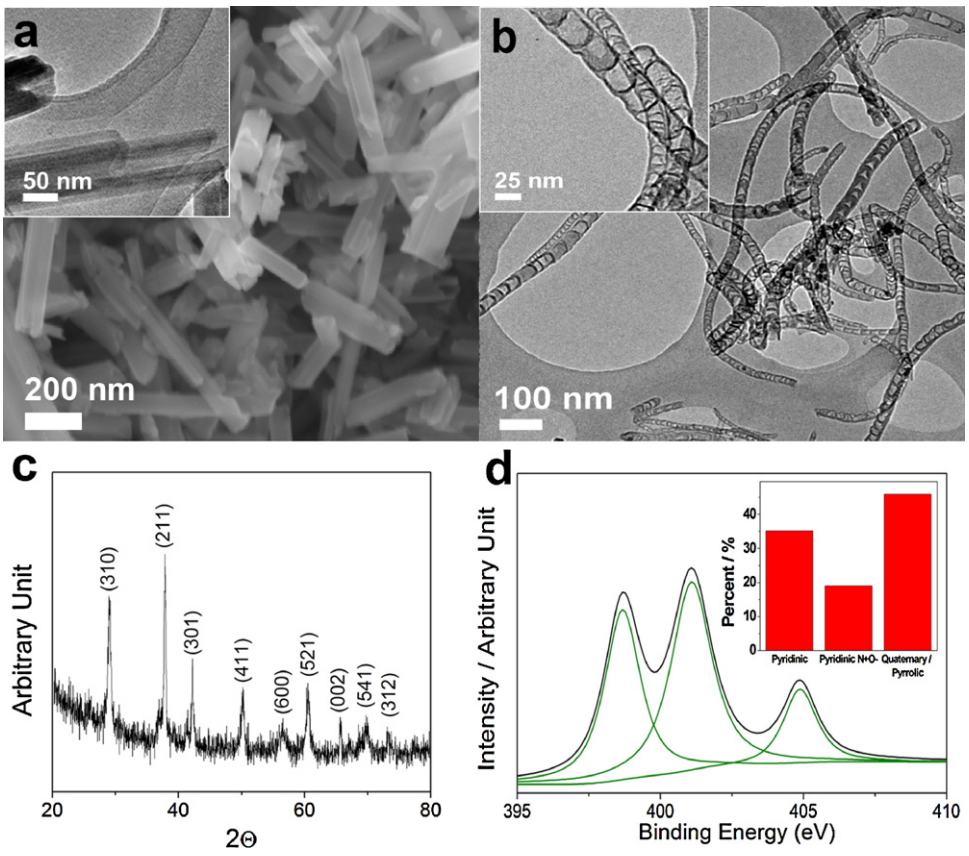

Fig. 1. Material characterization of MnO_2 nanotubes and NCNT, (a) SEM image of MnO_2 nanotubes, inset shows the TEM image of MnO_2 nanotubes, (b) TEM image of NCNT, (c) XRD pattern of MnO_2, and (d) deconvoluted high resolution XPS of the N1S signal of NCNT, inset shows the composition of the surface nitrogen groups.

where n is the number of electrons transferred, F is the Faraday constant, C_{O_2} is the bulk oxygen concentration, D_{O_2} is the diffusion coefficient of oxygen, and υ is the viscosity of the solution. Similar slopes are extracted from the K–L plots of the pure MnO_2 and the MnO_2–NCNT composite, which indicate first order reaction of ORR catalysis [31–33]. By extrapolation of K–L plot to the y-axis, the kinetic current density of different catalyst was determined. The kinetic current density at −0.55 V is 25 mA cm^{-2} for MnO_2–NCNT, approximately 10 times greater than that of pure MnO_2 (2.5 mA cm^{-2}). The results of K–L analysis further accentuate the beneficiaries of using MnO_2–NCNT composite as bifunctional catalysts for rechargeable zinc-air battery. More importantly, the substantial improvements in regard to both ORR and OER catalysis illustrate the effectiveness of the simple approach adapted in this work in creating composite bifunctional catalyst for rechargeable zinc-air battery.

Based on the promising data obtained from the half cell tests, battery evaluation of the pure MnO_2 and the MnO_2–NCNT composite was carried out. The polarization curves for battery discharge illustrates an activation loss region followed by a pseudo-linear ohmic loss region (Fig. 4a). Evidently, the MnO_2–NCNT composite exhibits lower ohmic loss compared to MnO_2. The lower ohmic loss experienced by the MnO_2–NCNT composite contributes to 62% improvement in discharge current density at 0.8 V. With respect to battery charging (Fig. 4a), similar current density was observed for the MnO_2–NCNT composite and the pure MnO_2. To further understand the electrode processes of the air electrodes, electrochemical impedance spectroscopy was performed. The Nyquist

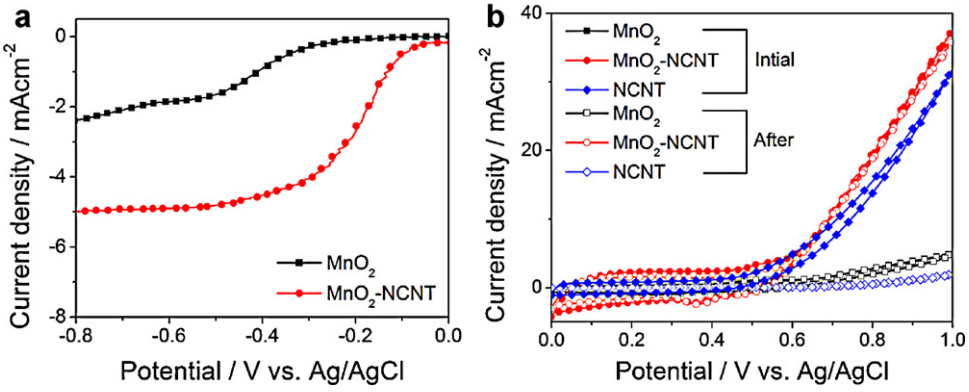

Fig. 2. RRDE voltammetry results showing (a) ORR polarization curves of the pure MnO_2 and the MnO_2–NCNT composite obtained at 900 rpm, and (b) OER polarization plot of the pure MnO_2, NCNT and the MnO_2–NCNT composite obtained at 900 rpm.

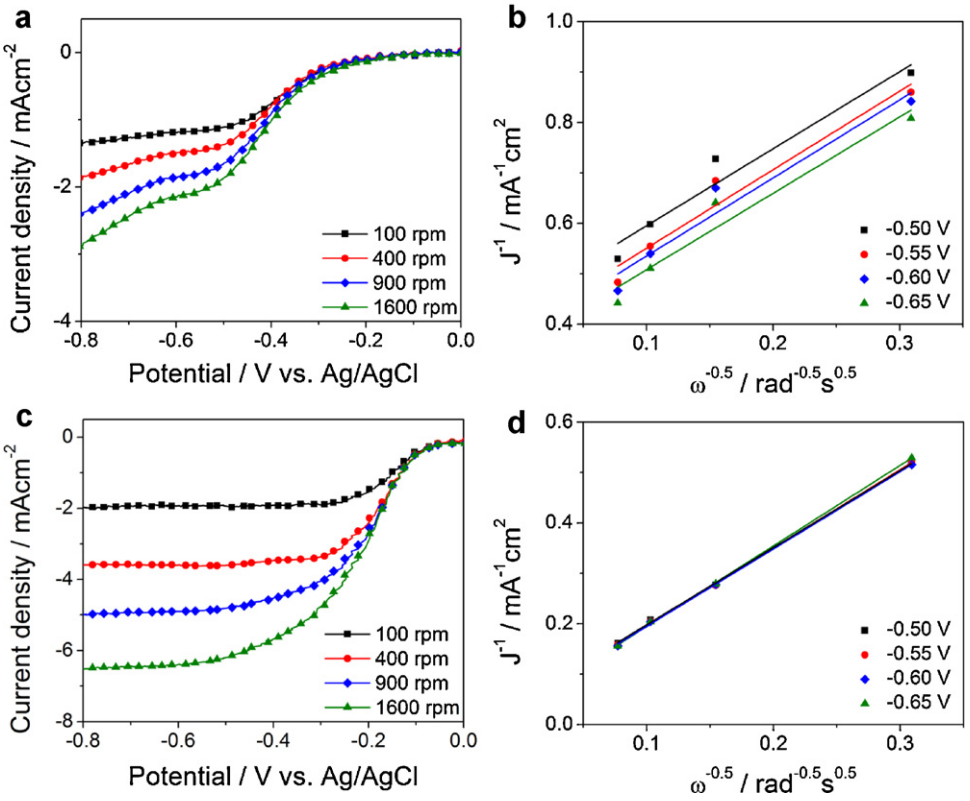

Fig. 3. ORR polarization curves of (a) the pure MnO_2, and (c) the MnO_2–NCNT composite. Koutecky–Levich plot of (b) the pure MnO_2, and (d) the MnO_2–NCNT composite.

plots of both catalysts illustrate two semicircles at high and low frequency regions (Fig. 4b). To identify the resistance and electrode processes of the battery, the impedance data was fitted using the equivalent circuit showed in Fig. 4b. Five elements are shown in the equivalent circuit, R_s, Q_{int}, R_{int}, Q_{dl} and R_{ct}. Similar equivalent circuit has been proposed by various researchers to investigate the electrode processes of the air electrode for zinc air battery [34,35]. The R_s component of the equivalent circuit represents the resistance associated with various battery components, such as the electrolyte and contact resistances. Additionally, the solid to electrolyte interface resistance can be present in the battery and is illustrated by R_{int}. Furthermore, R_{ct} represents the charge transfer resistance incurred during electrochemical reactions taking on the electrode [34,35]. The constant phase elements, Q_{int} and Q_{dl} are included in the equivalent circuit for modeling the non-faradaic processes in the battery. The constant phase elements are used in place of the conventional capacitance due to the use of porous electrodes as well as the non-homogeneity in the system. The Q_{int} refers to the capacitance arises from the solid electrolyte interface on the air electrode, and Q_{dl} represents the double layer capacitance [34,35]. Using the equivalent circuit, the value of the different electrochemical elements is extracted and summarized in Table 1. The value of R_s differs greatly for the two catalysts investigated, the MnO_2–NCNT composite displays much smaller overall battery resistance (by 34%) in contrast to the pure MnO_2. Compared with the pure MnO_2, the MnO_2–NCNT composite shows 50% smaller R_{ct}, which suggests more efficient ORR catalysis by the MnO_2–NCNT coated air cathode.

Building on the battery performance, the stability of pure MnO_2 and MnO_2–NCNT composite was investigated (Fig. 5) using charge–discharge (C–D) cycling. The upper potential regime of the

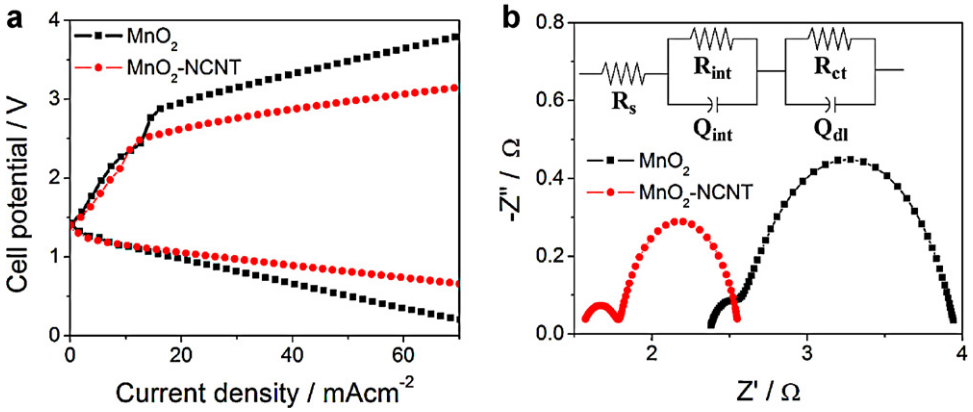

Fig. 4. Battery performances prior to C–D cycling, (a) battery discharge and charge polarization of the pure MnO_2 and the MnO_2–NCNT composite. (b) Nyquist plot of the pure MnO_2 and the MnO_2–NCNT composite, inset shows the equivalent circuit of the Nyquist plots.

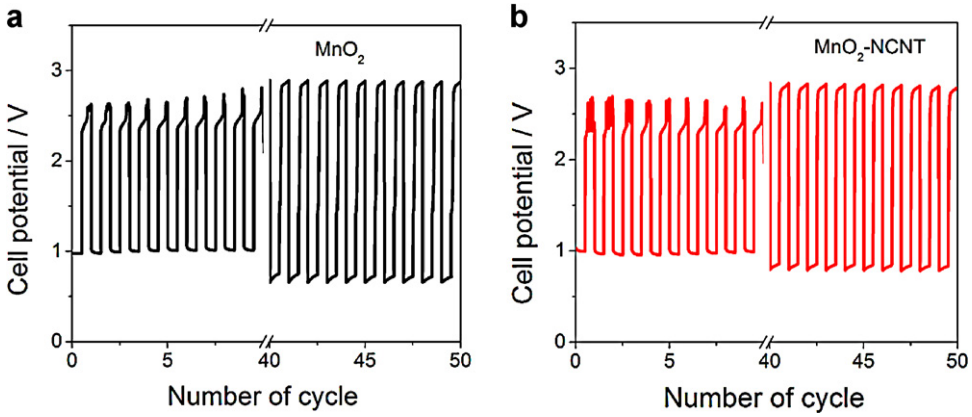

Fig. 5. Number of C–D cycles of (a) the pure MnO_2, and (b) the MnO_2–NCNT composite.

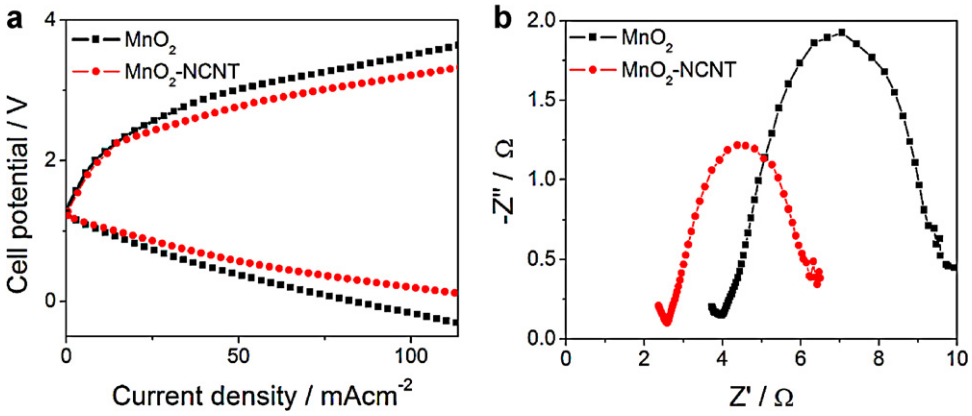

Fig. 6. Battery performances after C–D cycling, (a) battery discharge and charge polarization of the pure MnO_2 and the MnO_2–NCNT composite. (b) Nyquist plot of the pure MnO_2 and the MnO_2–NCNT composite.

C–D plot gauges the performance of the catalyst during charge. In this aspect, a smaller value is desirable as it indicates lower overpotential. The opposite is true regarding the lower potential regime of the C–D plot, which gauges the battery performance during discharge. For a highly stable catalyst, minimal fluctuation in the charge and discharge potential is required. The battery voltage during charge and discharge fluctuates greatly for the pure MnO_2, whereas the MnO_2–NCNT composite displays better stability. In particular, 10% and 31% change in charge and discharge potentials are observed for the pure MnO_2 (Fig. 5a). With respect to MnO_2–NCNT, the charge potential and discharge potential during C–D cycling varied by 5% and 20%, respectively (Fig. 5b). The relatively more stable C–D potentials displayed by MnO_2–NCNT directly indicate good recharge capability in addition to the outstanding ORR and OER activities displayed previously.

Battery discharge and charge were evaluated after C–D cycling (Fig. 6a). The MnO_2–NCNT composite illustrates superior performance repeatedly when compared to the pure MnO_2 in terms of charge and discharge current densities. Specifically, 36% higher current density was obtained for the composite bifunctional catalyst at 0.8 V and 2.5 V. Electrochemical impedance spectroscopy was performed to investigate the potential causes for performance decrease (Fig. 6b). As evident from the Nyquist plot of the pure MnO_2 and the MnO_2–NCNT composite, the impedance behaviours after cycling are significantly different from the initial results. The small depressed semi-circle present in the initial Nyquist plots no longer exists at the high frequency region. Meanwhile, the semi-circle associated with the charge transfer during the electrode reactions at the low frequency region persists after cycling. From the frequency dependent semi-circle, the value of R_{ct} and Q_{dl} can be estimated. Based on the new Nyquist plots, the value of R_{ct} for the MnO_2–NCNT composite is approximately 50% smaller compared to that of the pure MnO_2 after C–D cycling. The lower resistances of the MnO_2–NCNT composite after C–D cycling can be correlated with the higher battery performance. The superior electrical and electrochemical performance of the MnO_2–NCNT from impedance and the polarization data works in tandems to show that the MnO_2–NCNT composite is a better bifunctional catalyst than the pure MnO_2 nanotubes for rechargeable zinc-air battery. In addition, the distinctively superior performance of the MnO_2–NCNT composite is a testament to the effectiveness of the simple preparation method for the composite bifunctional catalyst investigated in this study.

Table 1
Equivalent circuit elements and their respective values for the air electrodes coated with the pure MnO_2 and the MnO_2–NCNT composite.

	MnO_2	MnO_2–NCNT
R_s	2.36	1.54
R_{int}	0.21	0.25
R_{ct}	1.38	0.77
Q_{int}	0.0024	0.0027
Q_{dl}	0.029	0.104

4. Conclusion

Successful preparation of the MnO_2 nanotubes, NCNT and the MnO_2–NCNT composite as well as the physiochemical and electrochemical characterizations were reported in this work. From half

cell and battery evaluations, the MnO_2–NCNT composite illustrates excellent bifunctional activity, and superior discharge, charge as well as cycling capability compared to MnO_2 nanotubes. The high ORR activity and electrical conductivity of NCNT can be correlated to the improved performance of MnO_2–NCNT composite observed thus far. This work demonstrates the potential application of the MnO_2–NCNT composite towards catalysis applications in rechargeable zinc-air batteries; and the feasibility of the simplistic synthesis of the bifunctional catalyst.

Acknowledgement

This research was supported by Natural Sciences and Engineering Research Council of Canada (NSERC) and the University of Waterloo.

References

[1] S.I. Smedley, X.G. Zhang, J. Power Sources 165 (2007) 897.
[2] V. Neburchilov, H.J. Wang, J.J. Martin, W. Qu, J. Power Sources 195 (2010) 1271.
[3] J. Goldstein, I. Brown, B. Koretz, J. Power Sources 80 (1999) 171.
[4] P. Sapkota, H. Kim, J. Ind. Eng. Chem. 15 (2009) 445.
[5] G.Y. Chen, D.A. Delafuente, S. Sarangapani, T.E. Mallouk, Catal. Today 67 (2001) 341.
[6] H. Liu, B.L. Yi, M. Hou, J.F. Wu, Z.J. Hou, H.M. Zhang, Electrochem. Solid State Lett. 7 (2004) A56.
[7] Y.M. Chang, P.W. Wu, C.Y. Wu, Y.C. Hsieh, J. Power Sources 189 (2009) 1003.
[8] M. Hamdani, R.N. Singh, P. Chartier, Int. J. Electrochem. Sci. 5 (2010) 556.
[9] Z. Chen, A. Yu, D. Higgins, Z.W. Chen, Nano Lett. (2012), doi:10.1021/nl2044327.
[10] L.Q. Mao, D. Zhang, T. Sotomura, K. Nakatsu, N. Koshiba, T. Ohsaka, Electrochim. Acta 48 (2003) 1015.
[11] F.Y. Cheng, Y. Su, J. Liang, Z.L. Tao, J. Chen, Chem. Mater. 22 (2010) 898.
[12] Y. Gorlin, T.F. Jaramillo, J. Am. Chem. Soc. 132 (2010) 13612.
[13] D.C. Higgins, J. Choi, J. Wu, A. Lopez, Z.W. Chen, J. Mater. Chem. 22 (2012) 3727.
[14] J. Choi, D.C. Higgins, Z.W. Chen, J. Electrochem. Soc. 159 (2012) B87.
[15] E. Antolini, Mater. Chem. Phys. 78 (2003) 563.
[16] K. Lee, J.J. Zhang, H.J. Wang, D.P. Wilkinson, J. Appl. Electrochem. 36 (2006) 507.
[17] D.C. Higgins, D. Meza, Z.W. Chen, J. Phys. Chem. C 114 (2010) 21982.
[18] M.S. Saha, R.Y. Li, X.L. Sun, S.Y. Ye, Electrochem. Commun. 11 (2009) 438.
[19] Z.W. Chen, D. Higgins, A.P. Yu, L. Zhang, J.J. Zhang, Energy Environ. Sci. 4 (2011) 3167.
[20] D.C. Higgins, J. Wu, W. Li, Z.W. Chen, Electrochim. Acta 59 (2012) 8.
[21] W. Li, A. Yu, D.C. Higgins, B. Llanos, Z.W. Chen, J. Am. Chem. Soc. 132 (2010) 17056.
[22] J. Choi, R.S. Hsu, Z.W. Chen, J. Phys. Chem. C 114 (2010) 8048.
[23] K.P. Gong, F. Du, Z.H. Xia, M. Durstock, L.M. Dai, Science 323 (2009) 760.
[24] H. Li, H. Liu, Z. Jong, W. Qu, D.S. Geng, X.L. Sun, H.J. Wang, Int. J. Hydrogen Energy 36 (2011) 2258.
[25] D.S. Geng, H. Liu, Y.G. Chen, R.Y. Li, X.L. Sun, S.Y. Ye, S. Knights, J. Power Sources 196 (2011) 1795.
[26] S.M. Zhu, Z. Chen, B. Li, D. Higgins, H.J. Wang, H. Li, Z.W. Chen, Electrochim. Acta 56 (2011) 5080.
[27] Z. Chen, D. Higgins, Z.W. Chen, Carbon 48 (2010) 3057.
[28] Z. Chen, D. Higgins, Z.W. Chen, Electrochim. Acta 55 (2010) 4799.
[29] C.C. Yang, S.T. Hsu, W.C. Chien, M.C. Shih, S.J. Chiu, K.T. Lee, C.L. Wang, Int. J. Hydrogen Energy 31 (2006) 2076.
[30] Z. Chen, D. Higgins, H.S. Tao, R.S. Hsu, Z.W. Chen, J. Phys. Chem. C 113 (2009) 21008.
[31] O. Solorza-Feria, S. Ramirez-Raya, R. Rivera-Noriega, E. Ordonez-Regil, S.M. Fernandez-Valverde, Thin Solid Films 311 (1997) 164.
[32] Z. Chen, J.Y. Choi, H.J. Wang, H. Li, Z.W. Chen, J. Power Sources 196 (2011) 3673.
[33] D. Higgins, Z. Chen, Z.W. Chen, Electrochim. Acta 56 (2011) 1570.
[34] G.Q. Zhang, X.G. Zhang, H.L. Li, J. Solid State Electrochem. 10 (2006) 995.
[35] D. Thiele, A. Zuttel, J. Power Sources 183 (2008) 590.